

Development of Ir(III)-Based Photocatalysts for NADH Oxidation and ROS-Mediated Cancer Phototherapy



Thesis submitted in partial fulfilment for the
Award of Degree

Doctor of Philosophy

By

Ashish Kumar Yadav

DEPARTMENT OF CHEMISTRY
INDIAN INSTITUTE OF TECHNOLOGY
(BANARAS HINDU UNIVERSITY)
VARANASI-221005
INDIA

Roll No. 21051007

2025

**Copyright ©
Department of Chemistry,
Indian Institute of Technology, Banaras
Hindu University, Varanasi 221005, India, 2025
All rights reserved.**

Dedicated to my

loving

Parents...

CERTIFICATE

It is certified that the work contained in the thesis titled “**Development of Ir(III)-Based Photocatalysts for NADH Oxidation and ROS-Mediated Cancer Phototherapy**” by **Mr. Ashish Kumar Yadav** has been carried out under my supervision and that this work has not been submitted elsewhere for a degree.

It is further certified that the student has fulfilled all the requirements of the Comprehensive Examination, Candidacy, and SOTA for the award of Ph.D. Degree.

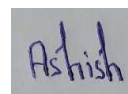
Samya Banerjee

Supervisor

DECLARATION BY THE CANDIDATE

I, *Mr. Ashish Kumar Yadav*, certify that the work embodied in this thesis is my own bona fide work and carried out by me under the supervision of **Dr. Samya Banerjee** from July 2021 to June 2025, at the *Department of Chemistry, Indian Institute of Technology (BHU), Varanasi*. The matter embodied in this thesis has not been submitted for any other degree/diploma award. I declare that I have faithfully acknowledged and given credit to the research workers wherever their works have been cited in my work in this thesis. I further declare that I have not willfully copied any other's work, paragraphs, text, data, results, etc., reported in journals, books, magazines, reports, dissertations, theses, etc., or available at websites and have not included them in this thesis and have not cited those as my work.

Date: 17/06/2025



Place: Varanasi

(Mr. Ashish Kumar Yadav)


CERTIFICATE BY THE SUPERVISOR

It is certified that the above statement made by the student is correct to the best of our knowledge.

Samya Banerjee

Supervisor

(Dr. Samya Banerjee)


विभागाध्यक्ष / HEAD
Signature of Head of
Department of Chemistry
Department/Coordinator of
School
Indian Institute of Technology (B.H.U.)
वाराणसी-221005 / Varanasi-221005

**"SEAL OF THE
DEPARTMENT/SCHOOL"**

COPYRIGHT TRANSFER CERTIFICATE

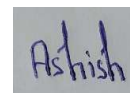
Title of the Thesis: Development of Ir(III)-Based Photocatalysts for NADH Oxidation and ROS-Mediated Cancer Phototherapy

Name of the Student: Mr. Ashish Kumar Yadav

Copyright Transfer

The undersigned hereby assigns to the Indian Institute of Technology (Banaras Hindu University), Varanasi, all rights under copyright that may exist in and for the above thesis submitted for the award of the "*Doctor of Philosophy*" degree.

Date: 17/06/2025



Place: Varanasi.

(*Mr. Ashish Kumar Yadav*)

Note: However, the author may reproduce or authorize others to reproduce material extracted verbatim from the thesis or a derivative of the thesis for the author's personal use, provided that the source and the Institute's copyright notice are indicated.

ACKNOWLEDGEMENTS

I want to express my truthful appreciation and heartfelt thanks to everyone around me for their valuable advice, criticism, commitment, and encouragement that made my journey conceivable.

Initially, I “*Mr. Ashish Kumar Yadav*” would like to express my deep sense of gratitude to my beloved mentor, guide and supervisor “**Dr. Samya Banerjee**”, Department of Chemistry, Indian Institute of Technology (Banaras Hindu University), Varanasi, for all brainstorming sessions, ideas, devoted time and energy. His extensive knowledge and ample experience always encouraged me throughout my academic research and daily life.

I sincerely acknowledge **Prof. Biplob Koch**, Banaras Hindu University, for his generous collaboration for biological assays. I am also profoundly grateful to **Dr. Arnab Dutta**, Indian Institute of Technology Bombay, for performing the single-crystal X-ray diffraction (SC-XRD) data collection. I also thank **Dr. Arpan Bera**, IISER Kolkata, for his kind assistance and contributions toward the biological studies.

I also express my heartfelt thanks to **Dr. Amit Kunwar** for his kind assistance in performing the in-cell NADH oxidation studies.

I want to thank my RPEC members, “Dr. Pandeewar Makam” and “Dr. Abhash Kumar Jha”, for their valuable suggestions, constant guidance, and kind encouragement during my research work.

I would like to sincerely thank Dr. Virendra Singh for performing the biological assays and for patiently explaining various biological concepts that were crucial to my research understanding. I also wish to express my gratitude to Mr. Sukanta Saha for carrying out the

single-crystal X-ray diffraction (SC-XRD) studies and for guiding me in learning and applying Olex2 software skills effectively.

My sincere thanks to the former Head of the department, “Prof. Dhanesh Tiwary and Prof. Yogesh Chandra Sharma, Department of Chemistry, IIT (BHU), Varanasi, and the present head, “**Prof. Sundaram Singh**” for their kind support and for extending all required facilities to carry out my research work.

I gratefully acknowledge the facilities provided by CIFIC-IIT (BHU), Varanasi, NMR facilities for characterization of samples, and Banaras Hindu University for HRMS facilities.

I want to express my deepest affection to my father, “**Mr. Rajnath Yadav**”, mother, “**Ms. Madhuri Yadav**”, and, sisters “**Ms. Pooja, Ms. Arti, Ms. Seema and Ms. Pinky**” for their love, concern, continuous moral support and encouragement which enabled me to perform my liabilities.

I want to extend my sincere thanks to “Dr. Arindam Indra”, Department of Chemistry, Indian Institute of Technology (Banaras Hindu University), Varanasi, for his guidance during the comprehensive and SOTA examinations.

I am deeply grateful to the “**Ministry of Education, Government of India**” for awarding me the **Prime Minister’s Research Fellowship (PMRF)**, which provided crucial financial support throughout my doctoral studies. I would also like to sincerely thank the **PMRF Evaluation Committee** for their consistent evaluation, feedback, and encouragement during the yearly review process.

I gratefully acknowledge the “Society of Biological Inorganic Chemistry (SBIC)” for providing generous travel support that enabled me to attend and present my research at the EuroBic-17 conference.

I am thankful to all my lab members “**Rajesh Kushwaha**”, “**Arif Ali Mandal**”, “**Apurba Mandal**”, “**Ishwar Singh**”, “**Shivam Pathak**”, “**Sagar Acharjee**”, “**Rohit Pandey**”, and “**Srijan Singh**”, for their kind co-operation and friendly environment during the entire period of my research.

I would like to warmly acknowledge the former junior members of our laboratory (**Souvik, Sumit, Ashish, Hemanto, Sameer, Arya**) for their enthusiastic support and assistance during various stages of my research.

Special thanks to our laboratory staff member, “**Mr. Ashish Kumar Maurya,**” for his support during my research.

Some special words of gratitude go to my friends who have always supported me when things get a bit discouraging: **Rajan, Arif, Apurba, Ravikant, Ishwar, and Nitin.** Thanks, guys, for always being there for me.

My special thanks to **Apurba Mandal** and **Ishwar Singh** for helping me till thesis submission.

My special thanks to **Rajesh Kushwaha** for his constant encouragement, timely help, and invaluable support throughout this journey. He has played a key role in helping me learn various experimental techniques and software skills.

It will be endless to list every friend, relative, and well-wisher who has directly or indirectly wished for my success in all endeavors. I thank one and all.

Date: 17/06/2025

(Mr. Ashish Kumar Yadav)
Research Scholar

Contents

Title	Page No.
CERTIFICATE	iii
DECLARATION BY THE CANDIDATE & CERTIFICATE BY THE SUPERVISOR	iv
COPYRIGHT TRANSFER CERTIFICATE	v
Acknowledgement	vi-viii
Contents	ix-xix
List of Figures	xx-xxxii
List of Schemes	xxxii
List of Tables	xxxiii-xxxiv
List of Symbols/Abbreviations	xxxv-xli
Preface	xlii-xliv
Chapter I: Introduction	1
1.1. Cancer	2
1.2. Cancer Cases Worldwide Statistics	3
1.3. Various Treatment Modalities Used in Cancer Treatment	4-5
1.4. Role of Chemotherapy in Cancer Treatment	5-6
1.4.1. Organic Molecule-Based Chemotherapeutic Drugs	6

Contents

1.4.2. Origin of Platinum-Based Chemotherapeutic Drugs	7-10
1.4.3. Drawbacks and Side Effects of Chemotherapy	10-11
1.4.4. Strategy to Overcome the Drawbacks of Chemotherapy	11-12
1.5. Photodynamic Therapy	12-13
1.5.1. Mechanism of Action	13-14
1.5.2. Organic Photosensitizers	14-15
1.5.3. Photosensitizers based on Transition Metal Complexes	15-16
1.5.4. Drawbacks of Photodynamic Therapy	16-17
1.6. Photocatalytic Cancer Therapy	17
1.6.1. Transition Metal-based Photocatalysts in Photocatalytic Cancer Therapy	18
1.6.2. Ir(III)-based Photocatalysts	18-30
1.7. Scope of Study and Objective of this Thesis	30-32
1.8. References	32-40

Contents

Chapter II: 2-Phenylpyridine Appended Phenanthroline-Based Cyclometalated Ir(III) Photocatalysts for NADH oxidation and ROS Mediated Cancer Phototherapy	41
2.1. Abstract	42-43
2.2. Introduction	43-44
2.3. Results and discussion	44
2.3.1. Synthesis and characterization	44-49
2.3.2. Solubility and Stability of 1-3	50
2.3.3. NADH photo-oxidation	50-54
2.3.4. Singlet oxygen generation	54-57
2.3.5. Photocytotoxicity	57-61
2.3.6. In-cell ROS generation	61-62
2.3.7. Mitochondrial depolarization	63-64
2.3.8. Cell death mechanism	64-67
2.3.9. Caspase 3/7 activation	68-70
2.4. Conclusions	70

Contents

2.5. Experimental section	71
2.5.1. Materials	71
2.5.2. Instruments	72
2.5.3. General synthetic procedure	72
2.5.4. Synthetic procedure of $[\text{Ir}(\text{C}^{\wedge}\text{N})_2\text{Cl}]_2$	73
2.5.5. General synthetic procedure for Photocatalysts (1-3)	73-76
2.5.6. NMR spectrometer	76
2.5.7. UV-visible spectroscopy	76
2.5.8. Fluorescence spectra	76
2.5.9. Photo-stability study	76
2.5.10. Photocatalytic reactions of 1-3 with NADH	77
2.5.11. Detection of H_2O_2 generation	77
2.5.12. Detection of singlet oxygen ($^1\text{O}_2$) generation	77-78
2.5.13. MTT assay	78-79
2.5.14. DCFH-DA assay	79

Contents

2.5.15. JC-1 assay	80
2.5.16. Apoptosis study by Hoechst 33342/PI dual staining	80-81
2.5.17. AO/EB dual staining	81-82
2.5.18. Annexin V-FITC/PI staining	82-83
2.5.19. Caspase 3/7 assay	83-84
2.5.20. Statistical analysis	84
2.6. References	84-89
Chapter III: Coumarin 6 Appended Phenanthroline-Based Cyclometalated Ir(III) Photocatalysts for NADH Oxidation and ROS-Mediated Anticancer Activity Under Normoxic and Hypoxic Conditions	90
3.1. Abstract	91-92
3.2. Introduction	92-94
3.3. Results and Discussion	94
3.3.1 Synthesis and Characterization	94-99
3.3.2. Electronic Spectra	100-101
3.3.3. Crystal Structure	101-103

Contents

3.3.4. Light Stability	103-104
3.3.5. DFT Calculation	104-108
3.3.6. NADH Photo-oxidation	108-113
3.3.7. In Solution ROS Generation	113-116
3.3.8. Photo-Cytotoxicity	116-123
3.3.9. Cellular Localization	124-125
3.3.10. In-cell NADH Oxidation	126-127
3.3.11. In-cell ROS Generation	127-128
3.3.12. Change in Mitochondrial Membrane Potential and Cellular Apoptosis	128-130
3.4. Conclusion	130-132
3.5. Experimental Section	132
3.5.1. Materials and General Instrumentation	132
3.5.2. Synthesis of Ir(III) μ -chloro-Bridged Dimer	132-133
3.5.3. Synthesis of 4-6	133-135

Contents

3.5.4. Instruments	135
3.5.5. NMR Spectroscopy	135
3.5.6. UV-Vis. Spectroscopy	135
3.5.7. Fluorescence Spectra	136
3.5.8. Photo-Stability of Photocatalysts	136
3.5.9. Single Crystal X-ray Crystallography	136-138
3.5.10. Computational Details	139
3.5.11. Photocatalytic Reactions of 4-6 with NADH	139-140
3.5.12. Cyclic Voltammetry	140
3.5.13. Detection of H ₂ O ₂ Generation	140
3.5.14. Determination of Singlet Oxygen Generation	140
3.5.15. Determination of Hydroxyl Radical Generation	140-141
3.5.16. MTT Assay	141
3.5.17. Sulforhodamine B (SRB) Assay	141-142
3.5.18. Confocal Microscopy	142-143

Contents

3.5.19. In-cell NADH Oxidation	143
3.5.20. DCFH-DA Assay	143-144
3.5.21. JC-1 assay	144
3.5.22. Annexin V-FITC/Propidium Iodide Assay	144
3.5.23. Caspase 3/7 Activity Assay	144
3.5.24. Statistical Analysis	144-145
3.6. References	145-149
Chapter IV: Coumarin 6 Appended Terpyridine-Based Cyclometalated Ir(III) Photocatalysts for NADH Oxidation and ROS-Mediated Anticancer Activity	150
4.1. Abstract	151
4.2. Introduction	151-153
4.3. Results and Discussion	153
4.3.1. Synthesis and Characterization	153-159
4.3.2. DFT Calculation	160-163
4.3.3. NADH Photo-oxidation	164-167

Contents

4.3.4. In-solution ROS Generation	167-170
4.3.5. Cellular Toxicity	170-175
4.3.6. Cellular Localization and In-cell NADH Oxidation	176-177
4.3.7. In-cell ROS Generation	177-178
4.3.8. Depolarization of Mitochondrial Membrane Potential (MMP)	179
4.3.9. Cell Death Mechanism	179-182
4.4. Conclusion	182
4.5. Experimental Section	183
4.5.1. Materials	183
4.5.2. General Synthetic Procedure	184
4.5.3. Synthesis of [Ir(Ph/An-tpy)Cl ₃]	184
4.5.4. Synthesis of [Ir(Ph/An-tpy)(CO ₆)Cl]Cl (7 and 8)	184-185
4.5.5. Instruments	186
4.5.6. NMR Spectroscopy	186
4.5.7. UV-Vis. Spectroscopy	186

Contents

4.5.8. Fluorescence Spectra	186
4.5.9. Lipophilicity Measurement	186-187
4.5.10. Photo-Stability of Photocatalysts	187
4.5.11. Dehalogenation Study of 7	187
4.5.12. Computational Details	187
4.5.13. Photocatalytic Reactions of 7/8 with NADH	187-188
4.5.14. Photocatalytic Reactions of 8 with NADH in the Presence of GSH (Glutathione)	188
4.5.15. Detection of H ₂ O ₂ Generation	188
4.5.16. Determination of Singlet Oxygen and [•] OH Generation	188
4.5.17. Determination of Hydroxyl Radical Generation in the Presence of [•] OH Scavenger	188-189
4.5.18. MTT Assay	189
4.5.19. Cellular Uptake	189
4.5.20. In cell NADH Oxidation	189
4.5.21. Intracellular ROS Generation	190

Contents

4.5.22. JC-1 Assay	190
4.5.23. Apoptosis Study by Hoechst/PI Dual Staining	190
4.5.24. Caspase 3/7 Activation Assay	190
4.5.25. Statistical Analysis	190-191
4.6. References	191-195
Summary, Conclusion, and Future Directions	196-204

List of Figures

Figure No.	Title	Page No.
Figure 1.1	A pictorial representation of normal cells and cancerous cells	2
Figure 1.2	(a) Worldwide estimated number of new cancer cases in males in 2020. (b) Worldwide, the estimated number of new cancer cases in females in 2020	4
Figure 1.3	Major Cancer Therapies	4
Figure 1.4	FDA-approved organic chemotherapeutic drugs	7
Figure 1.5	Pictorial representation of the mechanism of action of cisplatin	7
Figure 1.6	Structures of some FDA-approved Pt(IV) and Pt(II) based chemotherapeutic agents	10
Figure 1.7	Scheme of the steps involved in the NER mechanism	11
Figure 1.8	Schematic representation of different stages of PDT	13
Figure 1.9	Schematic representation of type I/II PDT	14
Figure 1.10	Structures of some FDA-approved Organic photosensitizers for PDT	15
Figure 1.11	Structures of metal-based photosensitizers that are either FDA-approved or in clinical trials	16
Figure 1.12	Structures of a few previously reported photocatalysts	18
Figure 1.13	Concentration of (a) NADH, (b) H ₂ O ₂ , and (c) ATP in A549 cells exposed to Ir1 under light (465 nm, 8.9 J/cm ²) or dark. (d)	20

List of Figures

	Increase in HMGB1 concentration after Ir1 +Light treatment, indicating immunogenic cell death	
Figure 1.14	Structures of Ir2-Ir5	22
Figure 1.15	(a) Structures of Ir6 and Ir7 . (b) SC-ICP-MS histograms showing the Ir-uptake in Ir7 (10 μ M)-treated HepG2 cells. (c) The bright green fluorescence of GFP after 48 hours of incubation with Ir7 in the FLK strain of zebrafish demonstrates Ir7 's biocompatibility. Scale bar: 500 μ m. (d) Images of tumors from mice bearing HepG2 cells under various treatment conditions, highlighting the <i>in vivo</i> effectiveness of Ir7 under light (525 nm, 88.68 J cm ⁻²)	23
Figure 1.16	Structures of Ir8 and Ir9	24
Figure 1.17	Structures of Ir10 and Ir11	25
Figure 1.18	(a) Structures of Ir12-Ir14 . (b) Catalytic cycle for NADH/NAD(P)H photooxidation by Ir14 under normoxia. (c) H&E staining and TUNEL assay images of colon tumor tissues from mice under different treatments show that the Ir14 +Light induces apoptosis	26
Figure 1.19	(a) Structures of Ir15-Ir20 . (b) Images showing that the Ir16 +Light significantly inhibited the growth of the A431 tumor in mice after 14 days. Light dose: 465 nm, 11.7 J/cm ²	27

List of Figures

Figure 1.20	Structures of Ir21-Ir24	29
Figure 1.21	Structures of Ir25-Ir27	30
Figure 2.1	Structures of (a) 1 , (b) 2 , and (c) 3	44
Figure 2.2	ESI-MS spectrum of (a) 1 , and (b) 2 in methanol. (c) HR-MS spectrum of 3 in methanol	45-46
Figure 2.3	¹ H NMR spectra of (a) 1 , (b) 2 , and (c) 3 in DMSO-d ₆ (500 MHz)	46-47
Figure 2.4	¹³ C NMR spectra of 1 in DMSO-d ₆ (125 MHz)	47
Figure 2.5	¹³ C NMR spectra of 2 in DMSO-d ₆ (125 MHz)	48
Figure 2.6	¹³ C NMR spectra of 3 in DMSO-d ₆ (125 MHz)	48
Figure 2.7	(a) Absorption spectra of 1-3 in DMSO:PBS (1:99 v/v) solution. (b) Emission spectra of 1-3 (50 μM each) in DMSO:PBS (1:99 v/v) [$\lambda_{\text{ex}} = 380 \text{ nm}$]	49
Figure 2.8	Photo-stability of (a) 1 , (b) 2 , (c) 3 (20 μM each) in DMSO:PBS (1:99, v/v) solution under visible light (400-700 nm, 10 J cm ⁻²) irradiation	50
Figure 2.9	Absorption spectra of NADH (175 μM) in the presence of (a) 1 , (b) 2 , (c) 3 (1 μM each) in DMSO: PBS (1:99, v/v) in the dark. (d) No significant change in absorption spectra of NADH (175 μM) in DMSO:PBS (1:99, v/v) under visible light (400-700 nm, 10 J cm ⁻²) irradiation, representing the necessity of photocatalysts for photo-oxidation of NADH	52

List of Figures

Figure 2.10	UV-Vis. absorption studies monitoring the light-induced NADH (175 μM) oxidation by (a) 1 , (b) 2 , and (c) 3 (1 μM each) in DMSO:PBS (1:99, v/v) solution under 400-700 nm light irradiation (10 J cm^{-2}). (d) Detection of H_2O_2 generation by 3 (1 μM) in the presence of NADH (175 μM) under light exposure (400-700 nm, 10 J cm^{-2}) using an H_2O_2 detection strip	53
Figure 2.11	Time-dependent absorbance changes of DPBF (50 μM) indicating $^1\text{O}_2$ generation in the presence of (a) 1 , (b) 2 , and (c) 3 (1 μM each) upon light irradiation (400-700 nm, 10 J cm^{-2}). Solvent: DMSO:PBS (1:99, v/v)	55
Figure 2.12	(a) No significant change in absorption spectra of DPBF (50 μM) only in DMSO:PBS (1:99, v/v) solution under visible light irradiation (Light source: 400-700 nm, 10 J cm^{-2}). Absorption spectra of DPBF (50 μM) in the presence of (b) 1 , (c) 2 , and (d) 3 (1 μM each) in DMSO:PBS (1:99, v/v) under dark conditions	56
Figure 2.13	Time-dependent absorbance changes of DPBF (50 μM) indicating $^1\text{O}_2$ generation in the presence of $[\text{Ru}(\text{bpy})_3]\text{Cl}_2$ (1 μM) upon light irradiation (400-700 nm, 10 J cm^{-2}). Solvent: DMSO:PBS (1:99, v/v)	57
Figure 2.14	Cell viability plots of 1-3 against A549 cells on (a) light exposure (400-700 nm, 10 J cm^{-2}) or (b) under dark treatment	59

List of Figures

Figure 2.15	Cell viability plots of the MTT assay in normal 3 -treated HEK-293 cells on light exposure (400-700 nm, 10 J cm ⁻²)	60
Figure 2.16	Intracellular ROS production by 3 (at light IC ₅₀ concentration) in A549 cells under dark and 10 J cm ⁻² light conditions (400–700 nm) was assessed using the DCFH-DA fluorescence probe.	62
Figure 2.17	MMP changes in A549 cells treated with 3 (at its light IC ₅₀ concentration), assessed using the JC-1 assay under dark and light conditions (L = light; D = dark)	63
Figure 2.18	(a) Apoptotic cell death induced by 3 (at light IC ₅₀ concentration) was evaluated through Hoechst 33342 and propidium iodide (PI) co-staining (L = light; D = dark). (b) AO and EB dual staining images of A549 cells collected from the control (dark and light) and 3 (at light IC ₅₀ concentration) under dark and light irradiation (400-700 nm, 10 J cm ⁻²) groups (L = light; D = dark)	65
Figure 2.19	Quantitative determination of the mode of cell death by 3 (at its light IC ₅₀ concentration) using flow cytometry using AnnexinV/PI assay (L = light; D = dark)	67
Figure 2.20	(a) The activation of caspase 3/7 was detected with cell event caspase-3/7 green detection reagent and SYTOX red in the presence of 3 (at its light IC ₅₀ concentration)+Light (400-700 nm, 10 J cm ⁻²) (L = light; D = dark). (b) Quantitative determination of	68-69

List of Figures

	the caspase 3/7 activation by 3 (at light IC ₅₀ concentration) using flow cytometry (L = light; D = dark)	
Figure 3.1	Structures of (a) 4 , (b) 5 , and (c) 6	94
Figure 3.2	ESI-MS spectra of photocatalyst (a) 4 in acetonitrile. HRMS spectra of (b) 5 and (c) 6 in acetonitrile	95-96
Figure 3.3	(a), (b) and (c) are ¹ H NMR spectra of 4-6 , respectively, in DMSO-d ₆ (500 MHz). (d), (e) and (f) are ¹³ C NMR spectra of 4-6 , respectively, in DMSO-d ₆ (125 MHz)	96-98
Figure 3.4	High-performance liquid chromatography (HPLC) spectra for analysis of photocatalysts (a) 5 and (b) 6	99
Figure 3.5	(a) Absorption spectra of photocatalysts 4-6 in DMSO. (b) Emission spectra of photocatalysts 4-6 (20 μM each) in DMSO:H ₂ O (1:9, v/v) [$\lambda_{\text{ex}} = 460 \text{ nm}$]	100
Figure 3.6	An ORTEP view of 4 with atoms labeling scheme	101
Figure 3.7	Unit cell packing diagram of 4	102
Figure 3.8	(a), (b), and (c) represent photo-stability of 4-6 , respectively, under exposure to white light (400-700 nm, 10 J cm ⁻²) at various time intervals in 0.5 % DMSO and 99.5 % PBS	104
Figure 3.9	The energy-optimized structures, HOMO, and LUMO of photocatalysts 4-6	105

List of Figures

Figure 3.10	Vertical energy levels of the different electronic states of 5 and 6 obtained from TD-B3LYP/LANL2DZ/6-31g* in water	106
Figure 3.11	(a), (b), and (c) Green light-induced NADH (240 μM) oxidation by photocatalysts 4-6 (2 μM each), respectively, monitored by UV-Vis. spectroscopy at different time intervals in 0.5% DMSO/99.5% PBS (v/v) solution (Light source: 525 nm, 50.2 J cm^{-2}). (d) The CV profiles of the 5 and 6 (1.0 mM each) in acetonitrile	109- 110
Figure 3.12	(a) Detection of H_2O_2 generation after irradiation of 1 min (Light source: 525 nm, 50.2 J cm^{-2}) for the reaction of photocatalyst 6 (2 μM) with NADH (240 μM) in 0.5% DMSO/99.5% PBS (v/v). (b) Detection of H_2O_2 generation after irradiation of various time intervals (Light source: 525 nm, 50.2 J cm^{-2}) for the reaction of photocatalyst 6 (2 μM) with NADH (260 μM) in 0.5% DMSO/99.5% PBS (v/v). (c) The concentration of NADH consumed vs irradiation time plot for 6 (2 μM) upon 525 nm light (50.2 J cm^{-2}) irradiation in 0.5% DMSO/99.5% PBS (v/v) solution	111
Figure 3.13	(a), (b) and (c) and (d) represent $^1\text{O}_2$ generation by photocatalysts 4/5/6/[Ru(bpy)₃]Cl₂ (2 μM each), respectively, in a 0.5% DMSO/99.5% PBS (v/v) solution as was detected with DPBF (50	114

List of Figures

	<p>μM) and monitored by UV-Vis. spectroscopy upon irradiation with 525 nm light (50.2 J cm^{-2}) at different time intervals. (e) Change in absorbance vs. irradiation time plot for 4-6, and reference $[\text{Ru}(\text{bpy})_3]\text{Cl}_2$ ($2 \mu\text{M}$ each) upon 525 nm light (50.2 J cm^{-2}) irradiation in 0.5% DMSO/99.5% PBS (v/v) solution</p>	
Figure 3.14	<p>Absorption spectra of DPBF ($50 \mu\text{M}$) in the presence of (a) 4, (b) 5, and (c) 6 ($2 \mu\text{M}$ each) in 0.5% DMSO/99.5% PBS (v/v) under dark conditions. (d), (e), and (f) represent $\cdot\text{OH}$ generation by photocatalysts 4/5/6 ($2 \mu\text{M}$ each), respectively, in a 0.5% DMSO/99.5% PBS (v/v) solution upon irradiation with 525 nm light (50.2 J cm^{-2})</p>	115- 116
Figure 3.15	<p>(a–c) Cell viability plots for photocatalysts 4–6 in A549, (d–f) HeLa, and (g–i) BEAS-2B cells</p>	117
Figure 3.16	<p>Cell viability plots for Cisplatin in normal human bronchial epithelial BEAS-2B cells</p>	119
Figure 3.17	<p>Cell viability plots using sulforhodamine B (SRB) assay for photocatalysts (a) 5 and (b) 6 in A549 cells. Cell viability plots for photocatalysts (c) 5 and (d) 6 under hypoxic conditions in A549 cells</p>	120
Figure 3.18	<p>Cellular localization study of photocatalyst 6 in A549 cancer cells</p>	125

List of Figures

Figure 3.19	(a) The plot shows the ratio of NAD ⁺ and NADH in A549 cells treated with photocatalyst 6 (25 μM) under dark and light. (b) Intracellular generation of ROS in A549 cells induced by 6 (1 μM) using DCFH-DA probe under dark and light	126
Figure 3.20	(a) Change in MMP by photocatalyst 6 (1 μM) treated A549 cells as monitored by JC-1 assay under dark and light. (b) Apoptotic death of A549 cells induced by 6 (1 μM) under dark and light (400-700 nm, 10 J cm ⁻²) was detected by annexin V-FITC/propidium iodide (PI) assay	128
Figure 3.21	The plot shows the activity levels of caspase 3 in A549 cells treated with photocatalyst 6 (25 μM) through spectrofluorometric analysis under dark and light	130
Figure 4.1	Chemical Structures of (a) 7 and (b) 8	153
Figure 4.2	HR-MS spectrum of (a) 7 , and (b) 8 in methanol	154
Figure 4.3	¹ H NMR spectra of (a) 7 , and (b) 8 in DMSO-d ₆ (500 MHz)	155-56
Figure 4.4	¹³ C { ¹ H} NMR spectra of (a) 7 , and (b) 8 in DMSO-d ₆ (125 MHz)	156- 157
Figure 4.5	(a) Absorption spectra of 7 and 8 in DMSO:PBS (0.5:99.5, v/v). (b) Emission spectra of 7 and 8 (20 μM each) in DMSO:PBS (0.5:99.5, v/v) [$\lambda_{\text{ex}} = 460 \text{ nm}$]	157

List of Figures

Figure 4.6	(a) Octanol-water partition coefficients of photocatalysts 7 and 8 . The UV-Vis. absorption spectra representing the green light stability of photocatalysts (b) 7 and (c) 8 , (d) The UV-Vis. absorption spectra of 7 and its dehalogenated species generated by AgNO ₃ treatment	158- 159
Figure 4.7	The optimized structures and HOMO, LUMO of 7 and 8	160
Figure 4.8	Vertical energy levels of the different electronic states of 7 and 8 , obtained from TD-B3LYP/LANL2DZ in water.	161
Figure 4.9	(a) and (b) represent green light (525 nm, 50.2 J cm ⁻²) induced NADH (150 μM) oxidation by 7 and 8 , respectively (1 μM each). Whereas (c) and (d) represent NADH (150 μM) oxidation by 7 and 8 , respectively (1 μM each) under dark conditions. Solvent: DMSO:PBS (0.5:99.5, v/v). (e) UV-Vis. spectra showing the green light (525 nm, 50.2 J cm ⁻²) induced NADH (150 μM) oxidation in the presence of 8 (1 μM) + GSH (50 μM). Solvent: DMSO:PBS (0.5:99.5, v/v). (f) H ₂ O ₂ generation was detected after 1 minute of green light irradiation (525 nm, 50.2 J cm ⁻²) to the 8 (1 μM) and NADH (150 μM) reaction mixture. Solvent: DMSO:PBS (0.5:99.5, v/v)	164
Figure 4.10	Absorbance changes of DPBF (50 μM) indicating ¹ O ₂ generation by (a) 7 and (b) 8 (2 μM each) upon 525 nm light irradiation. (c)	168

List of Figures

	Change in absorbance of DPBF (50 μM) vs irradiation time plot for 7 and 8 (2 μM each) upon 525 nm light (50.2 J cm^{-2}) irradiation. (d) No significant change in absorption spectra of DPBF (50 μM) in DMSO:PBS (0.5:99.5, v/v) under green light irradiation, representing green light (525 nm, 50.2 J cm^{-2}) stability of DPBF. The absorption spectra of DPBF (50 μM) in the presence of 7 (e) and 8 (f) (2 μM each) in DMSO:PBS (0.5:99.5, v/v) under dark conditions	
Figure 4.11	(a) Absorbance changes of DPBF (50 μM) in the presence of $[\text{Ru}(\text{bpy})_3]\text{Cl}_2$ (2 μM) with respect to time upon 525 nm light irradiation. Absorbance changes of methylene blue (15 μM) in the presence of (b) 7 and (c) 8 (2 μM each), indicating $\cdot\text{OH}$ generation under light irradiation (525 nm, 50.2 J cm^{-2}). (d) Absorption spectra of methylene blue (15 μM) in the presence of 8 (2 μM)+Light (525 nm, 50.2 J cm^{-2})+tert-butanol (8 μL)	169
Figure 4.12	Cell viability plots of 7 and 8 against MCF-7 cells under (a) dark and (b) light irradiation (400-700 nm, 5.0 J cm^{-2})	170- 171
Figure 4.13	Cell viability plots of 7 and 8 against HeLa cells under (a) dark and (b) light irradiation (400-700 nm, 5.0 J cm^{-2})	172- 173
Figure 4.14	Cell viability plots of 7 and 8 against HEK-293 cells under (a) dark and (b) light irradiation (400-700 nm, 5.0 J cm^{-2})	173- 174

List of Figures

Figure 4.15	(a) Fluorescence microscopy images showing the cytosolic localization of 8 in MCF-7 cells. (b) The plot displays the ratio of NADH/NAD ⁺ in MCF-7 cells treated with 8 (0.5 μ M) under dark and light	176- 177
Figure 4.16	(a) Detection of intracellular ROS generation in MCF-7 cells induced by 8 (at its light IC ₅₀ concentration) under exposure to visible light (400-700 nm, 5.0 J cm ⁻²) or under dark conditions using DCFH-DA probe (b) Change in the MMP of 8 (at its light IC ₅₀ concentration) treated MCF-7 cells as monitored by JC-1 assay after light exposure or in the dark	178
Figure 4.17	Hoechst and Propidium Iodide staining revealed that 8 (at its light IC ₅₀ concentration) caused light-activated apoptotic cell death in MCF-7 cells	180
Figure 4.18	Quantitative measurement of caspase 3/7 activation by staining with caspase-3/7 green detection reagent and SYTOX red under dark and light	181

List of Schemes

Scheme No.	Title	Page No.
Scheme 1.1	NADH oxidation photocatalytic cycle for Ir1 , (a) under normoxia, and (b) under hypoxia	19
Scheme 2.1	General synthetic pathway for $[\text{Ir}(\text{C}^{\wedge}\text{N})_2\text{Cl}]_2$ synthesis	73
Scheme 2.2	General synthetic pathway for the synthesis of 1-3	74
Scheme 3.1	Synthetic scheme of $[\text{Ir}(\text{CO})_2\text{Cl}]_2$	132
Scheme 3.2	Synthetic scheme of 4-6	133
Scheme 4.1	Synthetic scheme for the synthesis of 7 and 8	183

List of Tables

Table No.	Title	Page No.
Table 2.1	The TON and TOF of 1-3 and other Ir(III) based photocatalysts	53-54
Table 2.2	IC ₅₀ (μM) values of 1-3 against cancerous and normal cell lines and some selected Ir(III)-based photocatalysts	60-61
Table 3.1	Selected bond distances (Å) and bond angles (°) for [Ir(CO ₆) ₂ (phen)]Cl (4) with e.s.d.s in the parentheses	103
Table 3.2	Energy (eV) of the lowest vertical 10 singlet–singlet (S ₀ → S _n ; n = 1 to 10) transitions for the photocatalysts computed at the TD-B3LYP /LANL2DZ/6-31g* level of theory in water	106-107
Table 3.3	Energy (eV) of the lowest vertical 10 singlet–triplet (S ₀ → T _n ; n = 1 to 10) transitions for the photocatalysts computed at the TD-B3LYP /LANL2DZ/6-31g* level of theory in water	107-108
Table 3.4	Comparison of TON and TOF of 4-6 with other reported Ir(III) photo-catalysts for NADH photo-oxidation	112-113
Table 3.5	IC ₅₀ (μM) values of 4-6 and some selected Ir(III)-based photocatalysts under normoxia	121-122
Table 3.6	IC ₅₀ values of 5 and 6 against A549 cancer cells (determined by the SRB assay)	123
Table 3.7	IC ₅₀ (μM) values of 5 and 6 under hypoxic conditions (1% O ₂)	123-124

List of Tables

Table 4.1	Energy (eV) of the lowest vertical 10 singlet–singlet ($S_0 \rightarrow S_n$; $n = 1$ to 10) transitions of 7 and 8 computed at the TD-B3LYP /LANL2DZ/6-31g* level of theory in water	162
Table 4.2	Energy (eV) of the lowest vertical 10 singlet–triplet ($S_0 \rightarrow T_n$; $n = 1$ to 10) transitions of the 7 and 8 computed at the TD-B3LYP /LANL2DZ/6-31g* level of theory in water	163
Table 4.3	Comparison of TON and TOF of 7 and 8 with other reported Ir(III) photo-catalysts for NADH photo-oxidation	166-167
Table 4.4	IC ₅₀ (μ M) values of 7 , 8 , and some selected Ir(III)-based photo-catalysts	174-175

List of Abbreviations

μM	Micro Molar
$^1\text{O}_2$	Singlet Oxygen
2D	2-Dimensional
3D	3-Dimensional
$^3\text{O}_2$	Triplet Oxygen
5-ALA	5-Aminolevulinic acid
A431	Epidermoid Carcinoma Cell line
A549	Lung Cancer Cell
Abs	Absorbance
aip	2-(Anthracene-9-yl)-1H-imidazo[4,5-f][1,10]phenanthroline
An-tpy	4'-Anthracenyl-2,2':6',2''-terpyridine
AO	Acridine Orange
aq.	Aqueous
ATP	Adenosine Triphosphate
BEAS-2B	Normal Human Bronchial Epithelial
BN	Bombesin
<i>ca.</i>	Approximately
Calcd.	Calculated

List of Abbreviations

CCCP	Carbonyl Cyanide m-chlorophenyl Hydrazone
CHCl ₃	Chloroform
CNE-2Z	Human Nasopharyngeal Carcinoma
CO6	Coumarin 6
CPCM	Conductor-like Polarizable Continuum Model
DCF	2',7'-Dichlorofluorescein
DCFH-DA	2',7'-Dichlorodihydrofluorescein diacetate
DCM	Dichloromethane
DFT	Density Functional Theory
DMEM	Dulbecco's Modified Eagle Medium
DMF	Dimethylformamide
DMSO	Dimethyl sulfoxide
DNA	Deoxyribonucleic Acid
DPBF	Diphenylisobenzofuran
DPBS	Dulbecco's Phosphate Buffered Saline
dppz	Dipyrido[3,2-a:2',3'-c]phenazine
EB	Ethidium Bromide
EDTA	Ethylenediaminetetraacetic Acid
EPR	Electron Paramagnetic Resonance

List of Abbreviations

Equiv.	Equivalent
ESI-MS	Electrospray ionization mass spectrometry
<i>et al.</i>	And Others
Etc.	Et cetera
ETC	Electron Transport Chain
FACS	Fluorescence Activated Cell Sorting
FDA	Food and Drug Administration
Fe ³⁺ -cyt c	Fe ³⁺ -cytochrome c
FBS	Fetal Bovine Serum
FMO	Frontier Molecular Orbitol
GRPR	Gastrin-Releasing Peptide Receptor
GSH	Glutathione
H ₂ O	Water
H ₂ O ₂	Hydrogen Peroxide
HEK-293	Human Embryonic Kidney Cell Line
HeLa	Cervical Cancer Cell Line
HepG2	Liver Cancer Cell Line
HMGB1	High Mobility Group Box 1 Protein
HOMO	Highest Occupied Molecular Orbital
HPLC	High-Performance Liquid Chromatography
HRMS	High Resolution Mass Spectrometry

List of Abbreviations

HT-1197	Bladder Cancer Cell
ip	1H-imidazo[4,5-f][1,10]phenanthroline
IrCl ₃ ·xH ₂ O	Iridium(III) Chloride Hydrate
ISC	Inter System Crossing
J	Coupling Constant
J/cm ²	Joule/square centimeter
JC-1	5,5',6,6'-Tetrachloro-1,1',3,3'- tetraethylbenzimidazolylcarbocyanine iodide
LO2	Human Hepatocyte Cell Line
log <i>P</i>	lipophilicity
LUMO	Lowest Unoccupied Molecular Orbital
MB	Methylene Blue
MCF-7	Breast Cancer Cell Line
MDR	Multidrug Resistance
MeOH	Methanol
MHz	Mega Hertz
MLCT	Metal-to-Ligand Charge Transfer
MMP	Mitochondrial Membrane Potential
MRC-5	Human Lung Fibroblasts
MTR	Mitotracker Red

List of Abbreviations

MTT	3-(4,5-dimethylthiazol-2-yl)-2,5-diphenyltetrazolium bromide
MW	Molecular Weight
NADH	Nicotinamide Adenine Dinucleotide
NCI-H460	Lung Cancer Cell Line
NER	Nucleotide Excision Repair
NMR	Nuclear Magnetic Resonance
ns	Nanosecond
$O_2^{\cdot-}$	Super Oxide Radical anion
$\cdot OH$	Hydroxyl Radical
Obtd.	Obtained
PACT	Photoactivated Chemotherapy
PBS	Phosphate Buffer Saline
PC3	Prostate Cancer Cell Line
PCC	Pearson Correlation Coefficient
PCET	Proton-Coupled Electron Transfer
PCT	Photocatalytic Cancer Therapy
PDT	Photodynamic Therapy
phen	1,10-Phenanthroline
phip	2-Phenyl-1H-imidazo[4,5-f][1,10]phenanthroline

List of Abbreviations

Ph-tpy	4'-Phenyl-2,2':6',2''-terpyridine
PI	Photo Therapeutic Index
PI	Propidium Iodide
PS	Photosensitizer
Pt	Platinum
Pvt. Ltd	Private Limited
RNA	Ribonucleic Acid
ROS	Reactive Oxygen Species
rpm	Revolutions Per Minute
S ₀	Ground Singlet State
S ₁	Excited Singlet State
SAR	Structure Activity Relationship
SCE	Saturated Calomel Reference Electrode
SC-ICP-MS	Single-Cell Inductively Coupled Plasma Mass Spectrometry
SD	Standard Deviation
SGC-7901	Gastric Cancer Cell
SI	Selectivity Index
SK-OV-3	Human Ovarian Cancer Cell
SRB	Sulforhodamine B
T ₁	Triplet Excited State

List of Abbreviations

TCA	Trichloroacetic Acid
TD-DFT	Time-Dependent Density Functional Theory
tert-butanol	Tertiary Butanol
TLC	Thin-Layer Chromatography
TOF	Turnover Frequency
TON	Turnover Number
UV-Vis.	UV-Visible
<i>viz.</i>	Namely
WHO	World Health Organization
WST09	Padoporfin
γ -rays	Gama Rays
δ	Chemical Shift
$\Delta\Psi_m$	Mitochondrial Membrane Potential
ϵ	Molar Absorptivity Coefficient
λ_{em}	Emission Wavelength
λ_{ex}	Excitation Wavelength
τ	Excited State Lifetime

This thesis advances the photocatalytic cancer therapy field by introducing the different series of Ir(III) photocatalysts with enhanced NADH-oxidation photocatalytic performance and improved tissue-penetrating ability. The findings contribute to developing oxygen-independent anticancer strategies with significant potential for treating hypoxic tumors.

Chapter I of this thesis provides a comprehensive overview of cancer as a global health crisis. The chapter introduces various existing treatment modalities with their limitations. Finally, this chapter introduces the concept of photocatalytic cancer therapy (PCT) as a promising alternative to address these limitations. As this thesis is mainly based on Ir(III) based photocatalysts, this chapter gives a comprehensive overview of previously reported Ir(III) based photocatalysts, with a main focus on the reason behind their design and a detailed explanation of the anticancer mechanism. The chapter concludes by outlining the primary objectives of the research: to design and develop novel Ir(III) photocatalysts with red-shifted absorption, improved NADH oxidation activity, and effective intracellular performance, ultimately aimed at developing potent and selective agents for oxygen-independent cancer therapy.

Chapter II of this thesis presents the synthesis, characterization, in-solution light-induced NADH oxidation and ROS generation, photocytotoxicity in cancer cells, with a detailed study of the mechanism of cell death of three novel 2-phenyl pyridine appended phenanthroline-based Ir(III) photocatalysts.

Chapter III presents the synthesis, characterization, in-solution as well as in-cancer-cell photoinduced NADH oxidation, visible light assisted toxicity under both normoxic and

hypoxic conditions in different cancer cells, mode of photo-induced cell death, and cellular localization of three novel coumarin 6 appended phenanthroline based Ir(III) photocatalysts. The main objectives of this work are (i) to red shift the absorption wavelength of Ir(III) photocatalyst mainly in the green region, (ii) to enhance the photocatalytic performance, and (iii) to translate the light-induced in-solution NADH oxidation chemistry to inside the cancerous cell.

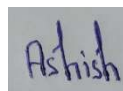
Chapter IV presents the synthesis, characterization, in-solution as well as in-cell photoinduced NADH oxidation, visible light assisted toxicity in different cancer cells and normal cells, mode of photo-induced cell death, and cellular localization of two novel coumarin 6 appended terpyridine based Ir(III) photocatalysts. The main objectives of this work are (i) to further enhance the photocatalytic performance, and (iii) to generalize the light-induced in-solution NADH oxidation chemistry in the presence of GSH.

Finally, **Chapter V** concludes the progress made in each chapter and provides future directions for the development of potential photocatalysts for photocatalytic cancer therapy. The references in the text have been indicated as superscript numbers and assembled at the end of each chapter. The photocatalysts presented in this thesis are represented by bold-faced numbers. Crystallographic data of the photocatalyst, which is characterized structurally by single-crystal X-ray crystallography, are provided in CIF format in the enclosed CD (Appendix I). Due acknowledgements have been made wherever the work described is based on the findings of other investigators. Any omission that might have happened due to oversight or mistake is regretted.

INDEX WORDS: Ir(III) photocatalyst · Crystal structure · High Turnover Frequency · In-cell NADH oxidation · Hypoxia active · Cellular Imaging. Apoptotic photocytotoxicity.

Date: 17/06/2025

Place: Varanasi



(Ashish Kumar Yadav)